The β Phase of Multiferroic Bismuth Ferrite and Its γ-β Metal-Insulator Transition

R. Palai[1], R.S. Katiyar[1], H. Schmid[2], P. Tissot[2],S. J. Clark[3], J. Robertson[4], S.A.T. Redfern[5] and J. F. Scott[5]
[1] *Department of Physics, University of Puerto Rico, San Juan, PR 00931-3343, USA*
[2] *Department of Inorganic, Analytical and Applied Chemistry, University of Geneva, CH-1211 Geneva 4, Switzerland*
[3] *Department of Physics, Durham University, Durham DH1 3LE, UK*
[4] *Department of Engineering, University of Cambridge, Cambridge CB2 1PZ, UK and*
[5] *Department of Earth Science, University of Cambridge, Cambridge CB2 3EQ, UK*
(Dated: February 1, 2008)

We have carried out extensive experimental studies, including differential thermal analysis, polarized and high-temperature Raman spectroscopy, high-temperature X-ray diffraction, optical absorption and domain imaging, and show that epitaxial (001) thin films of multiferroic bismuth ferrite ($BiFeO_3$) are monoclinic at room temperature instead of tetragonal or rhombohedral like bulk as reported earlier. We report a orthorhombic order-disorder β-phase between 820 and 950 ($\pm$ 5)°C contrary to the earlier report. The transition sequence rhombohedral-orthorhombic transition in bulk (monoclinic-orthorhombic in (001)$BiFeO_3$ thin film) resembles that of $BaTiO_3$ or $PbSc_{1/2}Ta_{1/2}O_3$. The transition to the cubic γ-phase causes an abrupt collapse of the bandgap toward zero (insulator-metal transition) at the orthorhombic-cubic β-γ transition around 950°C. Our band structure models confirm this metal-insulator transition, which is similar to the metal-insulator transition in $Ba_{0.6}K_{0.4}BiO_3$.

PACS numbers: 64. 70. Kb, 71. 30. +h, 78. 30. - j, 77. 55. + f, 77. 80. Bh

Magnetoelectric (ME) multiferroics are technologically and scientifically important because of their potential applications in data storage, spin valves, spintronics, quantum electromagnets, microelectronic devices *etc.* [1, 2, 3] and the novel mechanism that gives rise to electromagnetic coupling. Ferroelectricity originates from off-center structural distortions (d^0 electrons) and magnetism is involved with local spins (d^n electrons), which limits the presence of off-center structural distortion [4]. These two are quite complementary phenomena, but coexist in certain unusual multiferroic materials. $BiFeO_3$ (BFO) is one of the most widely studied multiferroic material because of its interesting ME properties *i.e* ferroelectricity with high Curie temperature ($T_c \approx$ 810-830 °C) [5] and antiferromagnetic properties below $T_N \approx$ 370 °C [5, 6]. The bulk BFO single crystal shows rhombohedral (a = 5.58 Å and $\alpha = 89.5^0$) crystal structure at room temperature (RT) with the space group R3c and G-type antiferromagnetism [6, 7]. If BFO were an ordinary antiferromagnet, the space group would be R3m [7]. The structure and properties of bulk BFO have been studied extensively [5, 6, 7, 8] and although early values of polarization were low due to sample quality, $P_r = 40\ \mu C/cm^2$ is now found in bulk by several different groups [9]. The weak ferromagnetism at room temperature occurs due to the residual moment from the canted spin structure [6]. It is very difficult to grow a high quality (defect free and stoichiometric) bulk single crystal with low leakage, which is detrimental to the practical applications of this material.

It has been found that thin films of BFO grown on (100) $SrTiO_3$ (STO) substrates show very high values of P_r (~55, 86, and 98 $\mu C/cm^2$ for the (001), (101), and (111) BFO films, respectively) and magnetization (M_r~150 emu/cc) [1, 10, 11]. (Very recently, Ricinschi *et al.* [12] have claimed P_r of 150 $\mu C/cm^2$ for the polycrystalline BFO films grown on Si substrates, but this is probably an artifact due to leakage and charge injection.) This makes BFO as one of the potential materials for the novel device applications, although the mechanism(s) behind the huge polarization claimed by some groups is not yet fully understood. Some experimental results [1, 10] and theoretical reports [13] suggest that the epitaxial strain might be the cause of such high value of P_r and M_r. However, a recent study showed that the epitaxial strain does not enhance M_r in BFO thin films [14]. It is believed that the heteroepitaxy induces significant and important structural changes in BFO thin films, which may lead to very high values for P_r.

There are some controversies in literature about the crystal structure of (001) epitaxial thin films. There have been several reports claiming tetragonal [1, 15], rhombohedral [11, 16], and monoclinic [17] structure of (001) BFO films on STO substrates. Therefore, the sequence of transitions is poorly understood, and there is no understanding of the overall physics of the phase transitions involved; more structural analysis of thin films is necessary for better understanding of engineered epitaxial and hetrostructure BFO thin films. In the present work we used a variety of techniques which combined show a sequence of transitions resembling the well-known 8-site model of barium titanate.

ABO_3 oxide perovskites which are rhombohedral at low temperatures, such as $LaAlO_3$, $PrAlO_3$, or $NdAlO_3$ [18, 19] have ferroelastic instabilities at the A-ion site that induce displacive phase transitions directly to cubic; but those which have B-site instabilities instead have order-disorder transitions to cubic that involve two or more steps. This has been successfully described [20, 21] by an eight-site model in which the B-ion displacements are always locally toward a [111] axis, but thermally average via hopping over [111], [$\bar{1}$11], [1$\bar{1}$1], and [11$\bar{1}$] to give orthorhombic, tetragonal, or cubic time- and space-

TABLE I: Selection rules for the Raman active modes for rhombohedral (R), tetragonal (T) and, monoclinic (M) crystal structures in different polarization configurations with total number of normal (N) Raman modes. The notation "<001>up" means unpolarized spectra along the pseudo-cubic <001> direction perpendicular to the substrate. The notation Z (along <001> direction) and $\bar{\text{Z}}$ are the directions of the incident and backscattered light, respectively.

Scattering geometry	R(R3c) (C_{3v})	$T(P4mm)$ (C_{4v})	$M(Bb)$ (C_s)
N(Raman)	$4A_1 + 9E$	$3A_1 + B_1 + 4E$	$13A^{'} + 14A^{''}$
<001>up	$4A_1 + 9E$	$3A_1 + B_1$	$13A^{'}$
Z(XX)$\bar{\text{Z}}$	A_1 and E	A_1 and B_1	$A^{'}$
Z(XY)$\bar{\text{Z}}$	E	No modes	$A^{'}$
Y(ZZ)$\bar{\text{Y}}$	A_1	A_1	$A^{'}$
Y(ZX)$\bar{\text{Y}}$	E	E	$A^{''}$

global averages. In the present work we show that this model describes BFO, contrary to conventional wisdom [22] but in agreement with NMR, which shows some B-site disorder [23].

A. The α-phase

The rhombohedral (R3c), tetragonal ($P4mm$) [1], and monoclinic (Bb)[24] structures of BFO give rise to 13, 8, and 27 distinct Raman-active modes, respectively, as listed in the Table I. For the orthorhombic distortion in the β-phase, as discussed below, the tetragonal entries will remain correct, with only a small splitting of the E-modes.

The Raman data for 300 nm thick (001)BFO thin film on the (100)STO substrate in the parallel, Z(XX)$\bar{\text{Z}}$ and perpendicular, Z(XY)$\bar{\text{Z}}$ polarization configurations reveal strong peaks at 74, 140, 172 and 219 cm^{-1}, while weaker peaks were observed at around 261, 370, 406, 478, 529, 609, 808 (very weak), 946, 1093 cm^{-1}. All of these peaks are due to the BFO normal modes of vibrations and none of them are arising from the substrate, contrary to the earlier reported Raman measurements [15, 25]. We verified our results using target materials and also growing (001)BFO films on different substrates. The existence of 13 identical peaks in both the Z(XX)$\bar{\text{Z}}$ and Z(XY)$\bar{\text{Z}}$ polarization configurations confirms the Raman selection rules for the monoclinic structure (see Table I) instead of tetragonal or rhombohedral as reported earlier[11, 15, 16]. This observation verifies the very recent report of monoclinic structure for the epitaxial BFO films grown on (001)STO substrates by Xu *et al.* [17] studied via synchrotron radiation. As the spectra along Y(ZZ)$\bar{\text{Y}}$ and Y(ZX)$\bar{\text{Y}}$ were heavily dominated by the scattering from the STO substrate, the contribution from the BFO film could not be separated. We looked very closely near the phase transition Temperatures. Two noticeable changes have been observed in the Raman spectra: disappearance of all stronger peaks (74, 140, 171 and 220 cm^{-1}) at $\sim$ 820 °C with the appearance of a few new peaks, and complete disappearance of spectra around 950 °C. This temperature behavior implies that the BFO maintains its room-temperature structure up to $\sim$ 820 °C indicating the ferroelectric-paraelectric (FE-PE) phase transition, in agreement with the earlier investigations on BFO bulk single crystal and polycrystalline [5, 22] samples. No evidence of soft phonon modes implies that the BFO has an order-disorder, first-order ferroelectric transition, unlike $PbTiO_3$. No decomposition was observed above 810°C contrary to the earlier studies [8], suggesting that our samples had fewer defects and dislocations.

B. The β-phase

The Raman spectra show that four lines ($\sim$ 213, 272, 820 and 918 cm^{-1}) persist above 820°C. In the cubic perovskite phase no first-order Raman lines are allowed; all ions sit at inversion centers, and all long wavelength phonons are of odd parity. The data show that the beta phase from 820°C to 950°C cannot be cubic as reported earlier [22]. Since our backscattering geometry with incidence radiation along Z-axis favors A_1 and B_1 phonons, four Raman modes ($3A_1 + B_1$) are predicted in the tetragonal (or orthorhombic) perovskite phase (Table I), in agreement with experiment. Small orthorhombic splitting of four unobserved E modes is predicted, but these modes are unobserved in the backscattering geometry. We observe no soft modes in these studies but some merely line-width increases, suggesting that the α-β and β-γ transitions are both order-disorder, compatible with the eight-site model originally developed by Comes *et al.* [20], and developed in detail by Chaves *et al* [21].

C. Thermodynamics of phases

The existence of a β-phase below the cubic γ-phase $\sim$930°C and below the decomposition point at 960°C has been known for some forty years [26], but the early Soviet work is rarely cited, and was sometimes considered not to be single-phase material. Using differential thermal analysis (DTA) in conjunction with high-temperature reflected polarized light microscopy, the $BiFeO_3$-Fe_2O_3 phase diagram of Speranskaya *et al.* [26] has been refined (Fig. 1). DTA thermograms shown in Fig. 2 illustrate the phase transformation sequence for both $BiFeO_3$ single crystals (small crushed dendrites) and thin film target materials.

These show four sharp endothermic peaks at around 823, 925, 933, and 961°C. They can be interpreted as: (a) a first-order α-β transition; (b) a β-γ transition; (c) peritectic decomposition of the cubic phase into flux and $Bi_2Fe_4O_9$; and (d) decomposition of $Bi_2Fe_4O_9$ into flux

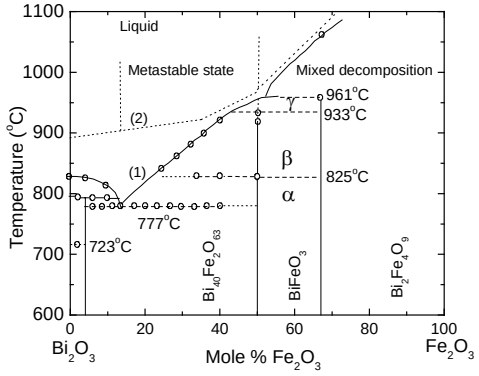

FIG. 1: Phase diagram of $BiFeO_3$. Open circles show the data points obtained by DTA. The DTA peaks were reversible below the solid line (line (1)) on cooling, while metastable states above the dotted line (line (2)). The α-phase is monoclinic in (001) thin film (rhombohedral in bulk), while the β and γ phases are orthorhombic and cubic, respectively.

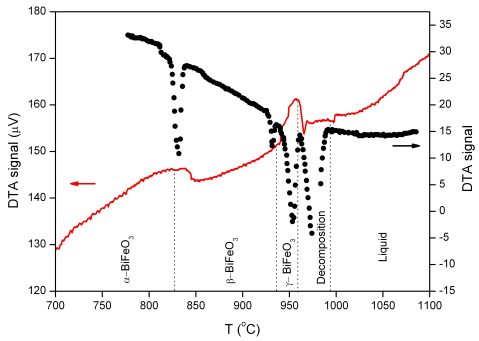

FIG. 2: DTA studies on crushed single crystal (dotted points) and thin film target material (solid line) of $BiFeO_3$. Signal has been inverted and offset for clarity.

and Fe_2O_3. The experimental values obtained on powders of crushed dendrites may be different for thin films, where transformations may be controlled by the build up strain energy. These DTA data and others for which the Bi/Fe ratio is varied produce the phase diagram shown in Fig.1.

High-temperature X-ray study of BFO powder (Fig.3) showed that the rhombohedral bulk structure has a strongly first-order transition near 825(± 5)°C to a P2mm orthorhombic structure. The unit cell volume shrinks by more than 1% upon heating through this transition from 64.05 (per formula unit) in the rhombohedral phase to 62.91 Å^3 in cubic. At around 925(± 5)°C there is a nearly second-order transition from orthorhombic to a cubic Pm3m phase. All of the phases have one formula group per unit cell, as in $BaTiO_3$. The rhombohedral cell parameter is $a = 4.0011$ Å. The orthorhombic cell parameters at 825(± 5)°C are $a = 3.9765(8)$ Å; $b = 3.9860(6)$ Å and $c = 3.9687(8)$ Å; and at 905°C $a = 3.9892(13)$Å; $b = 3.9926(9)$ Å and $c = 3.9848(9)$ Å. In the cubic

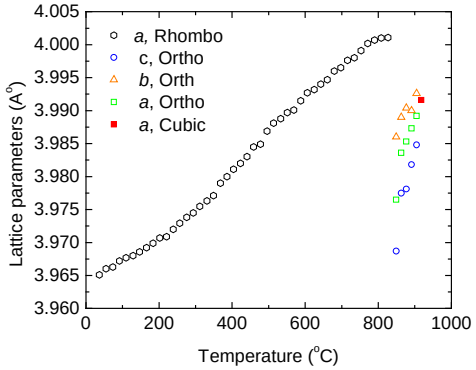

FIG. 3: Temperature variation of lattice parameters for rhombohedral (pseudo-cubic setting), orthorhombic and cubic phases of $BiFeO_3$. At 825°C the lattice constant $a = 4.0011$ Å splits into a triplet (open circles, squares, and triangles), which combines again at ca. 925(± 5)°C in the cubic phase (solid square), where $a = 3.9916$ Å.

phase $a = 3.9916(1)$Å at around 925(± 5)°C. The shortened bond length in the P2mm and Pm3m phases, compared with those in the rhombohedral phase, favors a metallic state. The sequence is similar to the other perovskite metal-insulator systems such as, $NdNiO_3$ and related rare-earth nickelates showing a sharp decrease of the unit-cell volume exactly at the metal-insulator transition [27].

D. Domains structures in $BiFeO_3$ single crystal

The Raman spectra do not discriminate between orthorhombic and tetragonal structures for the β-phase, but domain structures do. The orthorhombic domains that are symmetry-forbidden in tetragonal structures are too week to reproduce in Fig. 4, but in pesudo-cubic (pc) notion. They unambiguously rule out tetragonal structure for the beta-phase. The β-BFO phase has been recognized to be ferroelastic and non-cubic on the basis of microscopical observation of *ferroelastic* domains using reflected polarized light. The β-phase produces rectilinear ferroelastic domains and a clear phase boundary. On the basis of the ferroelastic domain pattern of the β-phase on a (111)pc-cut, showing rectilinear traces of both (100)pc and (110)pc walls, orthorhombic symmetry with axes parallel to <110> and <001> (analogous to $BaTiO_3$) is deduced, whereas a tetragonal phase would allow only (110)pc walls. The postulation of a cubic γ-phase in a very narrow temperature interval is based upon the reflected polarized light optical observation that the ferroelastic domains of the β-phase disappear at about 925°C, leaving the sample optically isotropic up to the decomposition point. Both types of domains can be seen in the photographs taken, but one cannot see rectilinear domain walls in the β-phase on this photo (Fig. 4). The ferroelastic nature of the α-β phase transition is nec-

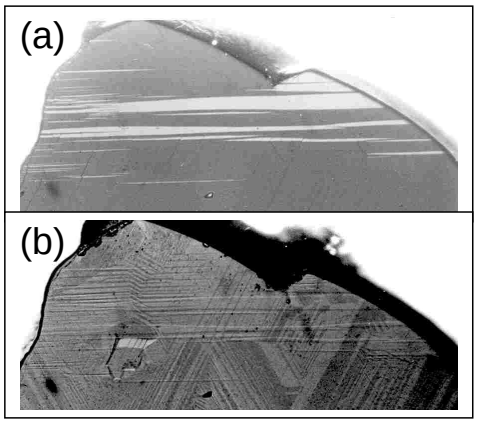

FIG. 4: Evolution of domain structure of β-phase of BFO with temperature; (a) at room temperature; (b) at 825°C with ferroelastic domains.

essary and sufficient to satisfy the Toledano [28] requirement that changes in crystal class are required for ferroelastic transitions (this treats rhombohedral and trigonal as a single super-class). Thus, for example, triglycine sulphate (TGS) with its monoclinic-monoclinic C_{2h}-C_2 transition cannot be ferroelastic.

E. The γ-phase

Visual observation shows [29] that bismuth ferrite single crystals at room temperature are yellow and transparent. The bandgap of BFO is calculated to be $E_g = 2.8$ eV [30] and usually measured experimentally as 2.5 eV. However, it has a large bandgap shift at the α-β phase transition temperature and turns deep red. If we define the band edge as where the absorption is 100 in 10 μm, then the experimental gap is 2.25, 2.18, 2.00 and 1.69 eV at 20, 160, and 300°C, respectively. But it shifts abruptly to 1.69 eV at 500°C, above which the E_g values are not yet known. There has been some controversy about its leakage current, with Clark *et al.* [30] showing that the ambient bandgap is too large for intrinsic mechanisms. Optical absorption shows that the bandgap decreases slowly and linearly with temperature in the α and β phases, from 2.5 eV to ca. 1.5 eV, but then drops abruptly to near zero at the β-γ transition near 930°C. Our observation is thus that E_g decreases significantly by the α-β transition temperature, and hence conduction in the high-temperature β-phase can be intrinsic. In the cubic γ-phase it is black and opaque. That is compatible with our band structure calculations (following section) that a non-cubic distortion is required to give it a finite bandgap.

Thus we regard β-BFO phase as semiconducting with small gap (calculated ∼1.5 eV) and γ-BFO phase from ∼930°C to ∼960°C as cubic and metallic; above 960°C decomposition occurs. The insulator-metal transition upon entering the cubic phase of BFO is very similar to that occurring in $Ba_{(0.6)}K_{0.4})BiO_3$ [31, 32] where the material becomes cubic and metallic. This implies in each case a strong electron-phonon interaction. The similarity with high-$T_c$superconducting cuprates in their normal states has been discussed [33]. The data graphed in this figure were obtained in two different ways: Below 830 K they were obtained by conventional absorption spectroscopy at a fixed temperature; but between 830 K and 1230 K they were obtained at a fixed wavelength (632.8 nm He-Ne) by slowly varying temperature and using the Urbach equation to relate absorption coefficient (a) to bandgap E_g(T): $log\ a(T) = (E - E_g)/E_g + constant$.

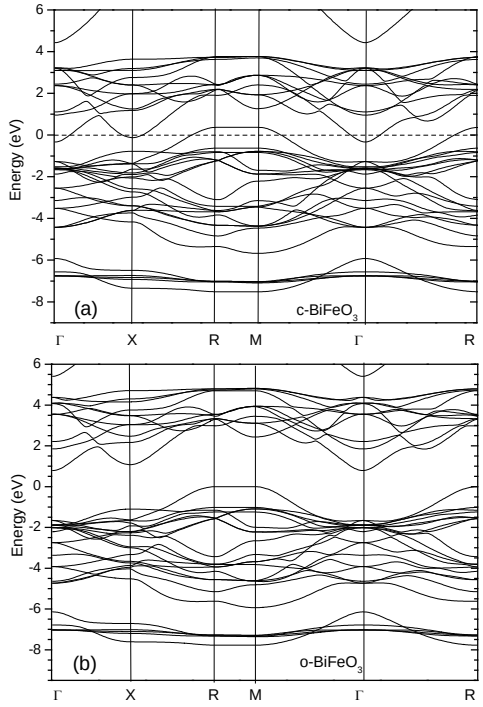

FIG. 5: Bandgap energy calculation for $BiFeO_3$ using screened exchange method for different structures; (a)cubic; (b) orthorhombic. Fermi level is at 0 eV in (a) and the valence band maximum is at 0 eV in (b).

The differences in transition temperatures between bulk and thin film, and single crystal, and also between the different studies drawn together in this paper, show that the transitions in the thin film are at higher temperatures than in the bulk material. The effect of pressure on these sorts of transitions is known, they have a negative dp/dT slope, as pressure stabilizes the higher symmetry phases in $BaTiO_3$. The thin film data would be consistent with this if you regard any surface relaxation or epitaxial strains in the thin films as imposing a negative pressure or lower density on the thin films. The large negative change in volume observed at the rhombohedral-orthorhombic transition in BFO is also consistent with the transition having a strong negative Clapeyron slope,

so surface relaxation might be expected to move the transition to higher temperature in the thin film.

F. Bandstructure model: Bandgap Collapse and Metal-Insulator Transition

Obtaining a band gap of zero is a common artifact in theoretical models using the local density approximation (LDA). Therefore, in the present study we circumvent this by using the screened exchange (sX) method [34]. This method is a density functional method based on Hartree-Fock, which includes the electron exchange via a Thomas-Fermi screened exchange term. It gives the correct band gap of many oxides, including antiferromagnetic NiO and rhombohedral $BiFeO_3$[30]. We find that the band gap of the cubic phase of BFO is indeed zero, as shown in Fig.5(a). The Fermi level lies within the Fe 3d states. It is interesting that in the cubic phase there is a direct gap at any point in the zone, and this opens up into a true band gap of 0.8 eV (calculated) in the orthorhombic phase as seen in Fig.5(b). Note that at RT the BFO has has an indirect band gap, but the direct gap lies only ca. 0.05 eV above it, and the valence band is very flat. Thus, with increasing T, as the conduction band descends, the gap can become direct.

G. Conclusion

In conclusion, high quality epitaxial (001)BFO films have been grown on (100)STO substrates using PLD. The XRD studies showed that films are *c*-axis oriented with high degree of crystallinity. The RT polarized Raman scattering of (001)BFO films showed monoclinic crystal structure contrary to the rhombohedral and tetragonal as reported earlier. The results obtained from DTA, high-temperature XRD, optical absorption, and polarized optics studies of domains were consistence. We observed the FE-PE structural phase transition at around 820°C no softening of Raman modes was observed at low frequencies. An intermediate β-$BiFeO_3$ phase between 820-950°C has been observed and recognized to be *orthorhombic* for the first time. The sequence of monoclinic(film)-orthorhombic-cubic phases or rhombohedral (single crystal)-orthorhombic-cubic in bulk; the phase sequence is extremely similar to that in $BaTiO_3$. Moreover, the transitions appear to be order-disorder from the Raman data, suggesting that the eight-site model of Comes *et al.* [20] and Chaves *et al.* [21] is applicable. We note that the high-T_c superconductor $Ba_{1-x}K_xBiO_3$ is also a perovskite oxide which becomes simultaneously cubic and metallic at x=0.4 [35]. This suggests a similar electron-phonon coupling; however, in the latter material the Bi-ion is at the B-site, whereas in $BiFeO_3$ it is at the A-site.

Acknowledgement

We thank W. Perez and Dr. M.K. Singh for experimental help. This work was supported by the DoD W911NF-06-0030 and W911NF-05-1-0340 grants and by an EU-funded project "Multiceral" (NMP3-CT-2006-032616) at Cambridge.

H. Method

BFO thin films of 300 nm thick were grown by pulsed laser deposition (PLD) using a 248 nm KrF Lambda Physik laser. Films were grown on STO(100) substrates of area $(5\ \text{mm})^2$ with ~ 25 nm thick $SrRuO_3$ (SRO) buffer layer. The growth parameters were as follows: substrate temperature of 700 °C, oxygen pressure of 10 mTorr, laser energy density of 2.0 J cm^{-2} at a pulse rate of 10 Hz, and a target-substrate distance of 50 mm. After the deposition, the chamber was vented with 0.4 atm of oxygen and then cooled at a rate of 30 °C/min to room temperature with an intermediate holding at 500°C for 20 min. The orientation, crystal structure and phase purity of the films were examined using Siemens D5000 X-ray diffractometer. The Jobin Yvon T64000 micro-Raman microprobe system with Ar ion laser (λ = 514.5 nm) in backscattering geometry was used for polarized and temperature depended Raman scattering. The laser excitation power was 2.5 mW and the acquisition time was 10 min per spectrum. The single crystal samples were made from crushed dendrites. The high-temperature X-ray data were collected from powdered bulk material using a Bruker D8-ADVANCE diffractometer with Cu-radiation, Göbel Mirror, and fast Vantec (linear psd) detector. Scans from 20 to 80^o 2θ were obtained every 15^o from 40^o to the decompostion point of BFO with an acquisition time of 8 min per pattern and a heating rate of 30°C/min between scans.

[1] Wang, J. *et al.* Epitaxial $BiFeO_3$ multiferroic thin film hetrostructures. *Science* **299**, 1719 (2003).

[2] Fiebig, M., Lottermoser, T., Fröhlich, D., Goltsev, A. V. & Pisarev, R. V. Observation of coupled magnetic and electric domain. *Nature* **419**, 818 (2002);

[3] Tokura, T. Multiferroic as quantum electromagnet. *Science* **312**, 1481 (2006).

[4] Hill, N. A. Why are there so few magnetic ferroelectrics. *J. Phys. Chem. B* **104**, 6694 (2000).

[5] Fischer, P., Polomska, M., Sosnowska, I. & Szymański, M. Temperature depedence of the crystal and magnetic structures of $BiFeO_3$. *J. Phys. C* **13**, 1931 (1980).

[6] Smolenskii, G. A. & Chupis, I. Ferroelectromagnets. *Sov. Phys. Usp.* **25**, 475 (1982).

[7] Kubel, F. & Schmid, H. Structure of ferroelectric and ferroelastic monodomain crystal of the perovskite $BiFeO_3$. *Acta Crystallogr. Sect. B: Struct. Sci.* **46**, 698 (1990).

[8] Bucci, J. D., Robertson, B. K. & James, W. J. The precision determination of the lattice parameters and the coefficients of thermal expansion of $BiFeO_3$. *J. Appl. Cryst.* **5**, 187 (1972).

[9] Shvartsman, V. V., Kleemann, W., Haumont, R. & Krisel, J. Large bulk polarization and regular domain structures in ceramic. *Appl. Phys. Lett.* **90**, 2115 (2007).

[10] Li, J. *et al.* Dramatic enhanced polarization in (001), (101), and (111) $BiFeO_3$ thin films due to epitaxial-induced transitions. *Appl. Phys. Lett.* **84**, 5261 (2004).

[11] Das, R. R. *et al.* Synthesis and ferroelectric properties of epitaxial $BiFeO_3$ films grown by sputtering. *Appl. Phys. Lett.* **88**, 242904 (2004).

[12] Ricinschi, D., Yun, K. & Okuyama, M. A mechanism for the 150 μC cm^{-2} polarization of $BiFeO_3$ films based on first-principle calculations and new structural data. *J. Phys: Condens. Matter.* **18**, L97 (2006).

[13] Ederer, C. & Spaldin, N. A. Influence of strain and oxygen vacancies on the magnetoelectric properties of multiferroics. *Phys. Rev. B* **71**, 224103 (2005).

[14] Eerenstein, W., Morrison, F. D., Dho, J., Blamire,M. G., Scott, J. F. & Mathur, N. D. Comment on "Epitaxial $BiFeO_3$ thin film hetrostructures". *Science* **307**, 1203a (2005).

[15] Singh, M. K., Ryu, H. & Jang, H. M., Polarized Raman scattering of multiferroic $BiFeO_3$ thin films with pseudo-tetragonal symmetry. *Phys. Rev. B* **72**, 132101 (2005).

[16] Qi, X. Dho, J., Tomov, R., Blamire, M. G. & J.L. MacManus-Driscoll, Greatly reduced leakage current and conduction mechanism in aliovalent-ion-doped $BiFeO_3$. *Appl. Phys. Lett.* **86**, 062903 (2005).

[17] Xu, G. *et al.* Low symmetry phase in (001) $BiFeO_3$ epitaxial constrained thin films. *Appl. Phys. Lett.* **86**, 182905 (2005).

[18] Scott, J.F. Raman study of trigonal-cubic phase transitions in rare-earth aluminates. *Phys. Rev.* **183**, 823 (1969);

[19] Geller, S. & Raccah, P.M. Phase transitions in perovskitelike compounds of the rare earths. *Phys. Rev. B* **2**, 1167 (1970).

[20] Comes, R., Lambert, M. & Guinier, A. Chain structure of $BaTiO_3$ and $KNbO_3$. *Solid State Comm.* **6**, 715 (1968).

[21] Chaves, A. S., Barreto, F. C. S., Nogueira, R. A. & Zẽke, B. Thermodynamics of an eight-site order-disorder model for ferroelectrics. *Phys. Rev. B* **13**, 207 (1976).

[22] Haumont, R., Kreisel, J., Bouvier, P. & Hippert, F. Phonon anomalies and the ferroelectric phase transition in multiferroic $BiFeO_3$. *Phys. Rev. B* **73**, 132101 (2006).

[23] Blinc, R. *Private communication*

[24] Ederer, C., & Spaldin, N. A. Weak ferromagnetism and magnetoelectric coupling in bismuth ferrite. *Phys. Rev. B* **71**, 060401(R) (2005).

[25] Singh, M. K., Jang, H. M., Ryu, S. & Jo, M. Polarized Raman scattering of multiferroic $BiFeO_3$ epitaxial films with rhombohedral R3c symmetry. *Appl. Phys. Lett.* **88**, 042907 (2006).

[26] Speranskaya, E. I., Skorikov, V. M., Rode, E.Y. & Terekhova, V. A. Phase diagram of the system of bismuth oxide-iron oxide. *Bull. Acad. Sci. USSR. Div. Chem. Sci.* (English Translation) **5**, 874 (1965).

[27] Gracía-Muñoz, J.L., Rodríguez-Carvajal, J., Lacorre, P. & Torrance, J.B. Neutron-diffraction study of $RNiO_3$ (R = La, Pr, Nd, Sm): electronically induced structural changes across the metal-insulator transition. *Phys. Rev. B* **46**, 4414 (1992).
Toledano, J. C. Theory of the ferroelastic transition in barium sodium niobate *Phys. Rev. B* **12**, 943 (1975).

[28] Toledano, J. C. Theory of the ferroelastic transition in barium sodium niobate *Phys. Rev. B* **12**, 943 (1975).

[29] Tabares-Munoz, C., Rivera, J. P. & Schmid, H. Ferroelectric domains, birefringence and absorption of single crystal of $BiFeO_3$. *Ferroelectrics 55*, 235 (1984);

[30] Clark, J. S. & Robertson, J. Band gap and Schottky barrier heights of multiferroic $BiFeO_3$. *Appl. Phys. Lett.* **90**, 132903 (2007)

[31] Cava, R. J., *et al.*, Superconductivity near 30 K without copper: The $Ba_{(0.6)}K_{(0.4)}BiO_3$ perovskite *Nature* 332, 814 (1988).

[32] Tajima, S., Yoshida M., Koshizuka N., Sato H., and Uchida S., "Raman-scattering study of the metal-insulator transition in $Ba_{(1-x)}K_{(x)}BiO_3$," *Phys. Rev. B* **46**, 1232 (1992).

[33] Sharifi, F., Pargellis A. & Dynes, R. C., Tunneling density of states in the lead-bismuth-oxide superconductors *Phys. Rev. Lett.* **67**, 509 (1991).

[34] Robertson, J, Xiong, K. & Clark, J. S. Band structure of functional oxides by screened exchange and weighted density approximation *Phys. Stat Solidi b* **243**, 2054 (2006)

[35] Anderson, P.W., New Physics of Metals: Fermi Surfaces without Fermi Liqwuids *Proc. Natl. Acad. Sci. USA* **92**, 6668 (1975).